The Eyjafjöll explosive volcanic eruption from a microwave weather radar perspective

F. S. Marzano[1,2], M. Lamantea[1], M. Montopoli[2,3], S. Di Fabio[2,4], E. Picciotti[4]

[1] Department. of Information Engineering, Sapienza University of Rome, Rome, Italy

[2] Centre of Excellence CETEMPS, University of L'Aquila, L'Aquila, Italy

[3] Department. of Electrical and Information Engineering, University of L'Aquila, Italy

[4] HIMET, L'Aquila, Italy

Correspondence to: F.S. Marzano (marzano@diet.uniroma1.it)

Submitted on 11 August 2011 to ***Atmospheric Chemistry and Physics (ACP),*** *Special issue on "Atmospheric implications of the volcanic eruptions of Eyjafjallajökull, Iceland 2010".*

Abstract

The sub-glacial Eyjafjöll explosive volcanic eruptions of April and May 2010 are analyzed and quantitatively interpreted by using ground-based weather radar data and the volcanic ash radar retrieval (VARR) technique. The Eyjafjöll eruptions have been continuously monitored by the Keflavík C-band weather radar, located at a distance of about 155 km from the volcano vent. Considering that the Eyjafjöll volcano is approximately 20 km from the Atlantic Ocean and that the northerly winds stretched the plume toward the mainland Europe, weather radars are the only means to provide an estimate of the total ejected tephra. The VARR methodology is summarized and applied to available radar time series to estimate the plume maximum height, ash particle category, ash volume, ash fallout and ash concentration every 5 minutes near the vent. Estimates of the discharge rate of eruption, based on the retrieved ash plume top height, are provided together with an evaluation of the total erupted mass and volume. Deposited ash at ground is also retrieved from radar data by empirically reconstructing the vertical profile of radar reflectivity and estimating the near-surface ash fallout. Radar-based retrieval results cannot be compared with ground measurements, due to the lack of the latter, but further demonstrate the unique contribution of these remote sensing products to the understating and modelling of explosive volcanic ash eruptions.

1 Introduction

The early detection and quantitative retrieval of volcanic ash clouds is both a scientific and practical issue which can have significant impacts on human activities. Volcanic eruptions can represent a serious socio-economic and a severe environmental hazard (Graf et al., 1999; Durant et al., 2010). Plume height, reaching typical altitudes of modern aerial routes, can affect flight safety and have huge knock-on effects on air traffic control, making necessary the re-routing of airways (Prata and Tupper, 2009). The volcanic eruptions may have both short-term effects, regarding health threats to people living in the area near the volcano, and long-term effects, since airborne ash clouds may affect both surface ocean biogeochemical cycles and control atmospheric feedbacks of climate trend (Robock, 2000; Duggen et al., 2010).

The previously described risk scenario has become unfortunately a reality in the spring 2010 during the last Eyjafjöll volcanic eruption which was the largest explosive eruption in Iceland since that of the Hekla volcano in 1947 (Petersen, 2010). The 2010 Eyjafjöll eruption featured both an initial phreato-magmatic phase (characterized by the presence of juvenile clasts, resulting from the interaction between magma and water) and predominantly magmatic remaining phases (Guðmundsson et al., 2010). Unlike previous Icelandic events, the 2010 Eyjafjöll eruption lasted several weeks, sustaining an average magma discharge of several hundred tonnes per second and producing large quantities of lapilli, coarse, fine and very fine ash particles which were advected towards south and south-east along the major European air traffic routes, causing an unprecedented flight crisis (Gertisser, 2010).

A quantitative measurement and analysis of volcanic ash cloud physical and chemical properties is crucial (Durant et al., 2010). Any decision support system for both civil protection and air traffic management needs not only a detection of the erupted and dispersed ash cloud, but also the estimation and forecast of its ash content (Prata and Tupper, 2009). The Eyjafjöll eruption on 2010 has been one of the best documented European volcanic events in terms of ground and satellite observations (e.g., Ansmann et al., 2010; Bennet et al., 2010; Flentje et al., 2010; Gasteiger et al., 2010; Guðmundsson et al., 2010; Madonna et al., 2010; Mona et al., 2010; Schumann et al., 2010; Pietruczuk et al., 2010; Stohl et al., 2011). Particular importance is devoted to the "near-source" (where the "source" is the volcano vent) instrumentation as measured data can be used to properly initialized ash-plume dispersion models (e.g., Bonadonna et al., 2009; Costa et al., 2006; Stohl et al., 1998). Coarse ash and lapilli are expected to fall within few hours from ejection time into air and within distances less than few hundreds of kilometres from the volcanic vent (Rose and Durant, 2009). This deposited tephra (i.e., the fragmental material produced by a volcanic eruption) is typically estimated to be more than 99% of the total ash mass (Wen and Rose, 1994). Advanced volcanic sites can deal with an ensemble of "near-source" synergetic instruments (Sparks et al., 1997; Zehner, 2010): *in situ* drillings and sondes, surveillance flights for plume monitoring, GNSS (Global Navigation Satellite System) differential receivers for deformation measurements, seismic signal receivers for tremor analysis, interferometric synthetic aperture radars (InSARs) for deformation imaging, ground-based lidars, ceilometers, photometers and microwave radars for plume probing, very-low-frequency (VLF) receivers for lightning detection and satellite infrared radiometers for broadscale plume tracking. Even unmanned airborne vehicles (UAVs) cannot be used to probe the near-source tephra due to inherent risks (Schumann et al., 2010). Satellite visible and thermal infrared split-window techniques may miss "near-source" tephra as they are basically insensitive to ash particles larger than few tens of microns (Yu et al., 2002; Pavolonis et al., 2006; Kahn et al., 2007; McCarthy et al., 2008; Stohl et al., 2010). On the other hand, ground-based optical "near-source" observations may be completely opaque due to the strong extinction of coarse and large ash particles (Zehner, 2010).

"Near-source" observations, if available, do not generally include estimates on the ash plume volume and concentration. The magma discharge estimate is primarily based on an empirical relationship established between observed eruption column heights, derived from ground-based weather radars, and magma discharge (Lacasse et al., 2004; Oddsson et al., 2009). Estimates on concentration of ash solid material in the eruption plume are usually based on theoretical assumptions, which may be supported by satellite-based observations of the ash cloud at mid to far distances (hundreds of kilometres) from the vent (Wilson, 1972; Sparks et al., 1997). In this context active microwave remote sensing, through ground-based scanning weather radars, can be better exploited and can represent a very powerful, and to some extent,

unique instrument to study explosive eruptions in proximity of volcanic vents (Harris and Rose, 1983; Lacasse et al., 2004; Marzano et al., 2006a; Gouhier and Donnadieu, 2008). In the "near-source" region weather radars may be capable to provide, in principle, not only the plume height, but also plume maximum height, ash particle category, ash volume, ash fallout and ash concentration (Marzano et al., 2006b, 2010a, 2010b, 2011a). Conventional weather radar targets are precipitating hydrometeors whose shape, dimension and dielectric properties are undoubtedly different from tephra ones (Sauvageot, 1992). This implies that weather radars cannot be used for ash cloud monitoring without developing ad hoc inversion methodologies and techniques to process radar data stream. Among these algorithms, the VARR (Volcanic Ash Radar Retrieval) approach has been shown to be a relatively general theoretical and operational framework to infer, in a quantitative way, ash mass category, concentration and fallout rate from three-dimensional (3D) scanning weather-radar measurements (Marzano et al., 2006b; 2010). The VARR products must be carefully treated as, any remote sensing inversion methodology, they are obtained under proper physical-statistical assumptions and given sensor limitations (e.g., receiver sensitivity and polarization agility).

The potential of VARR data processing in observing volcanic ash clouds, has been analyzed using some case studies where volcano eruptions happened near an available weather radar: i) the Grímsvötn volcano eruption in 2004, analyzed together with the Icelandic Meteorological Office (IMO) using a C-band weather radar (Marzano et al., 2006b, 2010, 2011a); ii) the Augustine volcano eruption in 2006, analyzed together with the US Geological Survey Alaska Volcano Observatory using an S-band weather radar (Marzano et al., 2010b). This work presents new results of the VARR methodology, applied to the sub-glacial explosive eruptions of Icelandic Eyjafjöll stratovolcano, whose maximum activities occurred on April and May 2010. The 2010 eruptions have been monitored and measured by the Keflavík C-band weather radar at a distance of about 155 km from the volcano vent (Guðmundsson et al., 2010). The distance between the Eyjafjöll volcano and the Icelandic coast is approximately 20 km. Due to the proximity between the volcano and the Atlantic Ocean and the prevailing northerly winds which stretched the plume toward the mainland Europe, collecting ground data samples in order to estimate the total ejected tephra or the ash distribution is not an easy task, especially in the nearby of the Eyjafjöll volcano. In this respect weather radar is one of the most powerful instruments to investigate this phenomenon and estimate the near-source ash fallout.

This paper is structured as follows. In section 2 the Eyjafjöll eruptions of April and May 2010 are described and the effects of the volcanic plume are summarized. Moreover, radar data are discussed and VARR algorithm data processing features are briefly introduced. In section 3 weather radar retrievals with reference to time and spatial volcanic cloud products are presented, discussed and compared. Lastly, section 4 is dedicated to conclusions and tracing future research and development perspectives.

2 Data and methodology

The Eyjafjöll stratovolcano is located under the Eyjafjallajökull ice cap, a small glacier within the Icelandic East Volcanic Zone (Larsen et al., 1998; Pedersen and Sigmundsson, 2006). The latter is the most active of the four Icelandic volcanic zones due to its position over the Mid-Atlantic Ridge, the divergent tectonic plate boundary between the Eurasian Plate and the North American Plate (Thordarson and Larsen, 2007). The eruptions in 2010 lasted several weeks, starting at the end of March with precursors event (such as seismic activities) since the

end of 2009; on April 2010 and May 2010 the activity of the volcano reached its peak levels, with some explosive eruptions (Guðmundsson et al., 2010; Petersen, 2010).

2.1 Volcanic eruptions on April and May, 2010

The Eyjafjöll eruptions in 2010 were preceded by seismic activities around December 2009 that increased at the end of February 2010 (Guðmundsson et al., 2010). These earthquakes were followed by the first magma pourings into the magma chamber of the volcano. In the first phase of the eruption, from March 20 to April 1, some fissures opened in Fimmvörðuháls (on the eastern flank of Eyjafjöll volcano) over the glacial ice. The eruption was rated, through the volcanic explosivity index (VEI, a relative logarithmic measure of the explosiveness of volcanic eruptions with value 0 for non-explosive eruptions and 8 for colossal ones), as VEI 1 due to the effusive, sub-glacial and weak volcanic activities and was precursory with respect to the second, more significant, eruption phase. The latter lasted from April 14 until May 20 and was rated VEI 4, thus being 40 times more powerful than the first phase (Guðmundsson et al., 2010).

On April 14 at 06:00 UTC, the Eyjafjöll volcano resumed erupting after a small hiatus; due to the main eruption site position under the centre of the glacier, the eruption became explosive and phreatomagmatic (Guðmundsson et al., 2010; Petersen, 2010). People living and working in the nearby areas were evacuated, in order to avoid potentially lethal encounters with the released glacier burst (or *jökulhlaup*, in Icelandic) and the large-scale discharge of melt water reaching the sand on the lowland plains (or *sandur*) to the north of the volcano. On April 15, the ash cloud reached mainland Europe, thus forcing the closure of airspace over a large part of the United Kingdom, Scandinavia and Northern Europe. The eruption tremors continued at a similar level to those observed immediately before the start of the second eruption phase. On April 16 and 17, a pulsating eruptive column reached above 8 km altitude, with a maximum of 13 km before the plume height decreasing to 5 km that was too low to let it travel across Europe. On April 18, the seismic activities continued, but the eruption further decreased (dropped by an order of magnitude) becoming magmatic (implying that external water no longer had ready access to the vents), with a maximum plume until 08:00 UTC lower than 3 km as recorded by the IMO. On April 19 the Eyjafjöll started to erupt lava flows that slowly melted their way through the ice of the Gígjökull outlet glacier and the plume reached again an altitude of 5 km, spreading to south direction due to northerly winds. On April 20, the GPS stations around Eyjafjallajökull showed a deflation associated with the eruption. In the following nine days, the eruption became discontinuous with increasing and decreasing tremors activities as reported by the IMO, and the ash plume rose up to few kilometres (often not exceeding the height of the cloud cover at about 5 km altitude) with mild explosive activity and light ash fall. During these first two weeks, continued, widespread and unprecedented disruption to flights and closure of some airports occurred both in Iceland and many European countries (Gertisser, 2010).

On the beginning of May, a lava producing phase larger than the explosive phase started. Plume became darker, denser and wider than in the preceding week, with an increased tephra fall out near the volcano and an eruption plume extended to altitudes between 4 km and 6 km (Guðmundsson et al., 2010; Petersen, 2010). On May 5 and 6, IMO stated that the volcano had entered a new phase with a shift back from lava to more ash production. An increase in explosive activity and considerable ash fall out was reported at a distance of about 70 km from the eruption site. Plumes were observed at altitudes between 5.5 km and 6.5 km, reaching a maximum height of 9 km. On May 7 and 8, the eruption was still in a strong explosive phase although its explosive activity decreased compared to the previous days: the

ash plume was rising to a lower altitude and was lighter in color. On May 9, the ash cloud reached its stretching maximum. In northern Spain (2.000 km from Iceland) and other western European countries (Ireland, France and Portugal), the ash cloud forced several airports closures. On May 10 the ash cloud rose up to between 5 km and 6 km (with some finer particles rising up to 9 km) and in the following days it became darker and was headed in a south-easterly direction. Since May 21, the eruptive vent emitted a column of steam (water vapour) plus sulphurous gases with an eruption column confined mostly in the proximity of the crater; no further report of any ash fall from the surrounding area have been registered. This phase of low activity and quiet state of the eruption was officially declared over on October.

2.2 C-band weather radar data

Weather radar systems, although designed to study hydrometeors and rain clouds, can be used to monitor and measure volcanic eruptions parameters (Harris and Rose, 1983; Marzano et al., 2006a). The measured radar backscattered power, from a volume bin at range r, zenith angle θ and azimuth angle φ, is proportional to the co-polar horizontally-polarized reflectivity factor Z_H [mm^{6}m^{-3}], which is expressed for an ensemble of spherical particles under the Rayleigh scattering assumption (Sauvageot, 1992):

$$Z_H(r,\theta,\varphi) = \frac{\lambda^4}{\pi^5 \mid K_\varepsilon \mid^2} \eta_H(r,\theta,\varphi) \cong \int_{D_1}^{D_2} D^6 N_{aX}(D) dD = m_6 \quad (1)$$

where λ is radar wavelength, K_ε is the particle dielectric factor (depending on its composition), η_H is the horizontally-polarized reflectivity, D is the equivolume spherical particle diameter, N_{aX} is the particle size distribution (PSD) and m_6 is the PSD sixth moment. The latter can be modelled as Scaled Gamma (X=SG) or Scaled Weibull PSD (X=SW), characterized by 3 parameters: the particle-number mean diameter D_n [mm], the ash concentration C_a [g/m^3] and the PSD shape coefficient μ (Marzano et al., 2006a; Sparks et al., 1997). From (1), keeping constant the ash particle distribution, the reflectivity factor Z_H tends to be higher for bigger particles. It is worth noting that the last approximation is not always valid as particle Mie backscattering effects may need to be taken into consideration depending on the ash cloud formation and the radar wavelength (Sauvageot, 1992; Marzano et al., 2006a). The measured reflectivity factor Z_{Hm} can be simulated from the theoretical one Z_H in (1) by introducing instrumental and model representativeness errors, the latter being usually modelled as a multiplicative zero-mean Gaussian noise (in linear units). Note that dual-polarization weather radars can offer the potential to measure not only Z_H, but also vertically-polarized reflectivity and differential phase shift which may be useful to better characterize ash particle properties and non-spherical shape (Marzano et al., 2011b). Weather radar volume samples, as in (1), are acquired by using discrete time and space steps. All radar-based retrieved geophysical parameters require the knowledge of data spatial and temporal resolution. Concerning the spatial resolution, the range bin size is proportional to the pulse width, whereas its transverse resolution quadratically increases with the radar range (Sauvageot, 1992). Temporal resolution is usually constant (here about 5 minutes) so that N_s radar volume scan temporal samples are available with sampling time step Δt_s, depending on the considered time interval.

The eruption was detected and monitored during its whole life span by the C-band (6 GHz) weather radar in Keflavík, located 155-km north-westwards far away from the caldera of Eyjafjöll volcano (e.g., Lacasse et al., 2004; Marzano et al., 2010). The Keflavík C-band radar

volumes were available from the IMO every Δt_s=5 minutes with reference to the two more significant time windows of the event: since 01:00 UTC (Universal Time Coordinated) on April 14, 2010 till 23:55 UTC on April 20, 2010 and since 00:10 UTC on May 05, 2010 till 23:55 UTC on May 10, 2010. Ten elevation angles were routinely available (specifically, 0.5°, 0.9°, 1.3°, 2.4°, 3.5°, 4.5°, 6.0°, 8.0°, 10.0° and 15.0°**).** The radar dataset consists of a total of N_s=3730 volumes in spherical coordinates with 10 elevation angles, 420 azimuth angles and 120 range bins, the latter having a range width of about 2 km.

Eight of the most significant Horizontal-Vertical Maximum Indicator (HVMI) recorded radar reflectivity images are shown in **Fig. 1** with reference to the time window of April and **Fig. 2** with reference to the time window of May. The maximum values of the detected reflectivity are projected on the surface as a PPI (Plan Position Indicator) geo-referenced radial map (right-bottom panel) and projected on two orthogonal planes along the vertical (top and left side of the HVMI image). The ash plume is visible over the Eyjafjöll, especially by looking at the upper section (showing the north-south profile of the plume) and the left section (showing the east-west profile of the plume). The detected volcanic cloud is distinguishable from undesired ground clutter and rain cloud returns, especially when looking at the HVMI vertical sections. Ground clutter can be easily recognized from HVMI as it tends to be stationary from an image to another. On the contrary, precipitating clouds have a reflectivity signature quite similar to ash clouds and the mix of the two is difficult to treat. In the case of 2010 Eyjafjöll event the observed temporal sequence indicates a distinct ash feature erupted from the volcano vent which can be effectively detected.

2.3 Weather radar data processing

The VARR approach foresees 2 steps: i) ash classification; ii) ash estimation. Both steps are trained by a physical-electromagnetic forward model, basically summarized by (1) where the main PSD parameters are supposed to be constrained random variables (Marzano et al., 2006b, 2010a). The generation of a simulated ash-reflectivity dataset by letting PSD parameters to vary in a random way, can be framed within the so called *Monte Carlo* techniques.

Automatic discrimination of ashes classes with respect to average diameter $<D_n>$ and with respect to average concentration $<C_a>$ implies the capability of classifying the radar volume reflectivity measurements into one of the N_c classes. In order to optimize and adapt the retrieval algorithm to the Icelandic scenario, VARR has been statistically calibrated with ground-based ash size distribution samples, taken within the Vatnajökull ice cap in 2005 and 2006 after the Grímsvötn last eruption occurred in November 2004 (Oddsson et al., 2009), since ground PSD data from the Eyjafjöll eruption are still quite limited (e.g., Stohl et al., 2010). Optimal values of PSD parameters have been adopted through best fitting of SG-PSD and SW-PSD on measured PSD for each ash diameter class (Marzano et al., 2011a). In summary, within each of the N_c=9 ash classes we have supposed a Gaussian random distribution for: i) D_n with average value $<D_n>$ equal to 0.006, 0.0641 and 0.5825 mm for fine, coarse and lapilli ash, respectively, a standard deviation $\sigma_{Dn}=0.2<D_n>$ and a corresponding variability of $0.001 \leq D_n < 0.06$ mm, $0.06 \leq D_n < 0.5$ mm, and $0.5 \leq D_n \leq 7.0$ mm; ii) C_a with mean value $<C_a>$ equal to 0.1, 1 and 5 g/m^3 for light, moderate and intense concentration regimes, respectively, and a standard deviation $\sigma_{Ca}=0.5<C_a>$. The ash density ρ_a has been put equal to an average value of 1200 kg/m^{-3}. The optimal PSD shape parameter μ has been set to 0.9, 1.1 and 1.4 for fine, coarse and lapilli particles. **Table 1** summarizes the modelled ash classes.

Within the VARR methodology, ash classification is performed by the use of the MAP (Maximum A Posteriori Probability) estimation (Marzano et al., 2006b). The probability density function (PDF) of each ash class (c), conditioned to the measured reflectivity factor Z_{Hm} can be expressed through the Bayes theorem. The MAP estimation of ash class, c, corresponds to the maximization with respect to c of the posterior PDF $p(c|Z_{Hm})$. Under the assumption of multivariate Gaussian PDFs, the previous maximization reduces to the following minimization which provides an ash class for a given volume bin centred in (r,θ,φ):

$$\hat{c}(r,\theta,\varphi) = Min_c\left\{\frac{[Z_{Hm}(r,\theta,\varphi) - m_Z^{(c)}]^2}{\left(\sigma_Z^{(c)}\right)^2} + \ln\left(\sigma_Z^{(c)}\right)^2 - 2\ln p[c(r,\theta,\varphi)]\right\} \quad (2)$$

where Min_c is the minimum value with respect to c, $m_Z^{(c)}$ and $\sigma_Z^{(c)}$ are the reflectivity mean and standard deviation of class c, whereas $p(c)$ is the a priori PDF of class c and the ash class perturbations have been assumed uncorrelated. Computing (2) requires knowledge of the reflectivity mean ($m_Z^{(c)}$) and standard deviation ($\sigma_Z^{(c)}$) of each ash class, c, derived from the 9-class simulated synthetic data set, previously described.

For each radar volume bin, the ash fallout rate R_a [kg m^{-2}s^{-1}] and ash concentration C_a [g m^{-3}] can be theoretically expressed by:

$$\begin{cases} R_a = \int_{D_1}^{D_2} v_a(D) m_a(D) N_{aX}(D) dD \\ C_a = \int_{D_1}^{D_2} m_a(D) N_{aX}(D) dD \end{cases} \quad (3)$$

where $v_a(D)$ is the terminal ashfall velocity in still air (when the vertical component of the air speed is neglected) and m_a is the actual ash mass particle (typically approximated by an equivolume sphere). A power-law dependence of v_a on D is usually assumed in (3), e.g. $v_a=a_vD^{b_v}$, as shown in Marzano et al. (2006b): from Harris and Rose (1983) the best fitting provides a_v=5.558 m/s and b_v=0.722, whereas from Wilson (1972) a_v=7.460 m/s and a_v=1.0.

The inversion problem to retrieve C_a and R_a from Z_{Hm} is ill-posed so that it can be statistically approached (Marzano et al., 2006b). Through the training forward model, as in (1), a regressive approximation may be used as a function of the class c for both C_a and R_a for a given volume bin centred in (r,θ,φ):

$$\begin{cases} R_a^{(c)}(r,\theta,\varphi) = c_c Z_{Hm}^{\ d_c}(r,\theta,\varphi) \\ C_a^{(c)}(r,\theta,\varphi) = a_c Z_{Hm}^{\ b_c}(r,\theta,\varphi) \end{cases} \quad (4)$$

where Z_{Hm} is the measured reflectivity factor and a_c, b_c, c_c and d_c are the regression coefficients, derived from simulated training dataset.

Sensitivity of weather radar observations to ash size and concentration is dependent on the transmitted wavelength and receiver minimum detectable signal (MDS), which in turn is quadratically dependent on the inverse range (Sauvageot, 1992; Marzano et al., 2006b). Numerical analysis has shown that intense concentration of fine ash (about 5 g/m^3 of average diameter of 0.01 mm) can be detected by a typical C-band radar 50 km far from the ash plume, whereas smaller concentrations are not usually retrieved (Marzano et al., 2006b). This limitation may be overcome, for the same transmitted power, by either reducing the range or increasing the receiver sensitivity or decreasing the wavelength or radially averaging data.

Another major problem is the incapability to discriminate between pure ash particles and aggregates of ash and hydrometeors (such as cloud ice and water) using single-polarization radar data only, as evident from Figs. 1 and 2. Apart from the use of *a priori* information, such as the freezing level and satellite-based imagery which are not always available (Marzano et al., 2010b), we can take into account these effects only as a larger uncertainty within the modelled Gaussian noise with a total standard deviation of 2.4 dBZ. A more robust VARR inversion algorithm will exhibit, of course, a larger estimate error variance.

3 Ash cloud retrieval

The VARR technique can be applied to each radar resolution volume in three-dimensional (3D) spherical coordinates where the measured C-band, $Z_{Hm}(r,\theta,\varphi)$, is larger than the minimum detectable reflectivity (MDZ), as discussed in Marzano et al. (2006b, 2010a). From the Keflavík radar specifications, at a range of about 155 km which corresponds to the Eyjafjöll volcano vent, MDZ is about -6 dBZ. From the mentioned analyses, this MDZ implies that radar echoes are sensitive to coarse ash and lapilli concentration, but not to moderate and light (< 5 g/m^3) fine ash distribution (Marzano et al., 2006b, 2010).

Only PPIs at the first 7 available elevation angles (i.e., 0.5°, 0.9°, 1.3°, 2.4°, 3.5°, 4.5° and 6.0°**)** have been used, as the other ones were useless since radar beam heights did not intercept the ash plume at higher elevations (see Figs. 1 and 2). Raw reflectivity data were averaged to about 2-km radial resolution in order to enhance the signal-to-noise ratio and thus reduce the MDZ. The VARR products in terms of ash concentration C_a and fallout R_a are originally provided within 3D spherical coordinates (r,θ,φ) reference system. Radar returns have then been geo-located into a new reference system (λ,ϕ,z) where λ is the longitude, ϕ is the latitude and z terrain height. Spherical coordinates have been converted into longitude and latitude through the inversion of the "haversine" formula, used to compute the great-circle distance (i.e. the shortest distance over the surface of the Earth) between two points:

$$\phi = \frac{180}{\pi}\left[\operatorname{asin}\left(\sin(\phi_R)\cos\left(\frac{r}{R_e}\right)\right)+\cos(\phi_R)\sin\left(\frac{r}{R_e}\right)\cos(\varphi)\right]$$
$$\lambda = \frac{180}{\pi}\left[\lambda_R\frac{180}{\pi}+\operatorname{atan2}\left(\sin(\varphi)\sin\left(\frac{r}{R_e}\right)\cos(\phi_R),\cos\left(\frac{r}{R_e}\right)-\sin(\phi)\sin(\phi_R)\right)\right] \quad (5)$$

where λ_R [decimal deg] and ϕ_R [decimal deg] are the Keflavík radar longitude and latitude in decimal degrees (respectively, -22.64° and 64.03°), asin is the arcsine function, atan2 is the four quadrant inverse tangent (arctangent) function and 180/π converts radians into decimal degrees. Supposing a standard atmosphere for electromagnetic waves propagation, the terrain altitude z can be derived by:

$$z = \sqrt{r^2 + R_e^{\,2} + 2rR_e\sin(\theta)} - R_e + z_R \quad (6)$$

where z_R [m] is the radar height above sea level (47 m in our case) and R_e= (4/3) R_T is the equivalent Earth radius, given by the so called "4/3 refraction model", where R_T [km] is the Earth radius (Sauvageot, 1992). The relation (6) states that the radar beam height is range and elevation angle dependent: when r and θ increase, the detected altitudes increase so that only some of the elevation angles can be used due to the large radar-volcano distance and the expected maximum plume heights. A finer grid (λ,ϕ,z) has been generated in order to allow an easier data geolocation.

3.1 Retrieval time series

The instantaneous volcanic ash cloud volume $V_a(t)$ [m^3], which represents the volume of the ash cloud at a given time step t (the latter is referred to as "instantaneous" even though the radar employs about 2 minutes to complete a volume scan), may be estimated by using a threshold C_{ath} on the estimated concentration $C_a(\lambda,\phi,z;t)$ at a given position (λ,ϕ,z) as follows:

$$V_a(t) \equiv \int_{C_a(\lambda,\phi,z;t)\geq C_{ath}} dV \tag{7}$$

where dV [m^3] is the elementary volume. The radar-derived total volume V_{aT} [m^3] can then be computed by integrating $V_a(t)$ with respect to the initial and final time steps of the volcanic eruption.

The instantaneous volume $V_a(t)$ in (7) should be, indeed, distinguished into the "detected" volume $V_{ad}(t)$ and a "hidden" (non-detected) volume $V_{ah}(t)$ (e.g., see Figs. 1 and 2). In general $V_a(t)=V_{ad}(t)+V_{ah}(t)$ due to the radar observation geometry and the presence of occlusions along the ray paths. The term V_{ah} implies that the total portion of the ash cloud $V_a(t)$ may not be detectable by the scanning radar, thus inducing an underestimation of the total ash volume and mass. This problem, which is clearly visible in Figs. 1-2 by looking at HVMI horizontal and vertical projections and is worse at larger distances, is a well known problem in radar meteorology and it is often overcome relying on the reconstruction of the vertical profile of reflectivity (VPR) (Sauvageot, 1992; Marzano et al., 2004). An approximate way to approach the VPR problem is to project the measured reflectivity Z_{Hm}, available at the lowest range bin, down to the terrain height at $z=z_s$, assuming that the lowest detectable value is the major responsible of ash fallout deposited on the ground from the vertical column above a considered position. To some extent, this approach is similar to that adopted when estimating the total mass from satellite thermal-infrared radiometers when estimates of ash cloud top layers are extrapolated to ground (Wen and Rose, 1994; Yu et al., 2002). In both approaches we are neglecting the finite time interval that a radar resolution volume (bin) of ash takes to reach the ground (given an ash terminal velocity). Note that the latter, coupled with the horizontal transport effects, may cause a displacement between the radar measure and the actual ash deposition at the ground.

Using $V_a(t)$, the instantaneous ash mass $M_a(t)$ [kg], from each radar 3D volume, is given by:

$$M_a(t) \equiv \int_{V_a(t)} C_a(\lambda,\phi,z;t)dV = \rho_a V_a(t) \tag{8}$$

where ρ_a [kg/m^3] is the ash density assumed to be constant and equal to about 1200 kg/m^3. The temporal trend of the instantaneous total mass $M_a(t)$, retrieved from VARR and defined in (7), is shown in **Fig. 3** with reference to both available datasets on April and May 2010. The instantaneous volume temporal trends, obtained from (7), are shown in **Fig. 4** for the same time windows as in Fig. 3.

These plots are useful to estimate the intensity of the volcanic eruption in near real-time mode. The scan sampling period is equal to 5 minutes so that the time series shows a time window of about 10020 minutes (equal to 167 hours) since the first available radar measurements at 01:00 UTC on Apr 14, 2010 with reference to the dataset of April and about 8630 minutes (equal to 143.8 hours) since the first available radar measurements at 00:10 UTC on May 5, 2010 with reference to the dataset of May. Both Figs 3 and 4 shows that the eruption peak on April 2010 was at the beginning of the 16th day where ash mass up to $15\cdot10^8$ kg was estimated. During the May episode the most intense day was on May 5 with ash mass

up to $8 \cdot 10^7$ kg. It is interesting to note: i) the intermittent and pulsed temporal character of the Eyjafjöll eruption, especially during the April volcanic activity; ii) the abrupt decrease of erupted mass at the end of April 16; iii) the longer and gradually decrease tail of the May event which lasts more than 6 days.

The spatial distribution of the instantaneous maximum plume height $H_a(\lambda,\phi;t)$ [km] can be then derived by using either a threshold Z_{Hmth} on the measured reflectivity $Z_{Hm}(\lambda,\phi,z;t)$ or a threshold C_{ath} on $C_a(\lambda,\phi,z;t)$ as follows:

$$H_a(\lambda,\phi;t) \equiv \begin{cases} Max_z\left[z \mid Z_{Hm}(\lambda,\phi,z;t) \geq Z_{Hmth}\right] \\ Max_z\left[z \mid C_a(\lambda,\phi,z;t) \geq C_{ath}\right] \end{cases} \quad (9)$$

where Max_z is the maximum operator with respect to z. The two approaches do not necessarily provide the same result, as will be shown later, due to the different and independent adopted thresholds. The maximum height H_{aM} of $H_a(\lambda,\phi;t)$ with respect to any (λ,ϕ) in (9) is provided by:

$$H_{aM}(t) \equiv Max_{\lambda,\phi}\left[H_a(\lambda,\phi;t)\right] \quad (10)$$

where $Max_{\lambda,\phi}$ is the maximum operator with respect to (λ,ϕ). The maximum height, H_{aM}, can be also referred to the spatial sub-domain around the volcano vent. The analysis of the maximum plume height H_{aM} is both an important input parameter in a plenty of volcanological models which forecast the volcanic eruption intensity and the most useful quantity to aerial routes planning in the areas near the volcanic eruption (Stohl et al., 2010). Plinian and sub-Plinian explosive eruptions reach their neutral level (above this height the cloud stops its vertical growth and starts to spread radially) at the same altitude of modern commercial airplanes flight level (Sparks et al., 1997). The merging of local VAACs (Volcanic Ash Advisory Centres) information with the information about the plume height, estimated by meteorological forecast centres, can be very useful to produce more accurate and precise VA-SIGMET (Volcanic Ash SIGnificant METeorological event information) reports (Prata and Tupper, 2009).

The temporal evolution of the maximum plume height H_{aM}, during a time interval from 01:00 UTC on April 14, 2010 till 23:55 UTC on April 20, 2010 and from 00:10 UTC on May 05, 2010 till 23:55 UTC on May 10, 2010 is shown in **Fig. 5**, with 5-minute resolution. The two plots show the estimates of VARR algorithm with detection thresholds on concentration ($C_a > 10^{-3}$ g/m^3) with reference to April (upper panel) and May (lower panel) eruptions. All the altitudes are scaled with reference to the Eyjafjöll height above sea level (1666 m). **Fig. 6** shows the same of Fig. 5, but by using (9) with a detection thresholds on reflectivity ($Z_{Hm} > -6$ dBZ). The plume height estimation shows a certain variability, also due to the altitude discrete sampling of radar beams at given elevations. Indeed, the degraded radial resolution (about 2 km in our case) should not be confused with the minimum step for estimating H_a or H_{aM}. The radar radial resolution coincides with the vertical resolution only for antenna zenithal pointing (or elevation angle equal to 90°). For low elevation angles, such as those of scanning weather radars, the vertical coordinate z in (9) is resolved at a variable range-dependent resolution which, in our case, may be even less than few hundreds of meters. For both eruption periods the estimated maximum height is up to 10 km, with a larger dynamical range of values for the April event than for the May event. It is worth noting that the temporal trend of $H_{aM}(t)$ is not necessarily correlated with the estimated $M_a(t)$.

The maximum plume height retrievals H_{aM}, provided by weather radars, can be used as an input variable in models that compute the eruption discharge rate (EDR), a useful parameter

to mark the intensity of a volcanic eruption (Wilson, 1972; Sparks et al., 1997). The thermal energy of the erupted tephra is used to heat the air trapped within the eruption jet and causes convective phenomena that raise the eruptive column. When the EDR is known, it is possible to estimate the thickness of the ash layer that will settle on the ground according to a model widely used for eruption columns which produce strong plumes (Wilson et al., 1978). Adapting the Morton relation to the Eyjafjöll volcano eruption (Morton et al., 1952) and considering a basaltic magma the estimated EDR, indicated by $Q_H(t)$ [m^3/s], can be obtained from maximum plume height through the following approximate relation (Oddsson et al., 2009; Marzano et al., 2011a):

$$Q_H(t) \cong 0.085\left[H_{aM}(t)\right]^4 \tag{11}$$

The relation (11) shows that EDR is linked to the fourth power of the height and so small fluctuations of the height cause large variations of the EDR. EDR temporal trends, obtained from VARR using (11) with a threshold on ash concentration C_a, are shown for both April and May time windows in **Fig. 7**. The power-law dependence of Q_H on the maximum plume height tends to amplify the EDR peaks. This figure suggests that the larger EDR is on April 14 and across April 17, with an isolated peak on April 19, 2010. The behaviour on May is more uniform with some relative maxima on May 5 and 6, 2010.

The EDR can be also directly evaluated from the temporal trend of the estimated ash volume $V_a(t)$. The radar-derived EDR $Q_V(t)$ [m^3/s] is evaluated through the ratio between the temporal average instantaneous volume and the sampling interval Δt:

$$Q_V(t) = \frac{\overline{V_a(t)}}{\Delta t} = \frac{1}{\Delta t}\left(\frac{1}{\Delta t}\int_0^{\Delta t} V_a(t)dt\right) \cong \frac{V_a(t_i)}{\Delta t_s} \tag{12}$$

where t_i is the *i-th* time step within the sampling period Δt_s where V_a is assumed constant in order to obtain the approximation of $Q_V(t)$ in (12). Similarly to Fig. 7, **Fig. 8** shows the estimated $Q_V(t)$ using (12) for both the April and May periods. The temporal trend of $Q_V(t)$ is quite different from that of $Q_H(t)$, shown in Fig. 7. The reason of this difference may be attributed to the fact that Q_H takes into account only the ash cloud altitude, whereas Q_V is related to the erupted 3D volume. Indeed, the estimate of $Q_V(t)$ is affected by the observation geometrical limits which reduce the detected $V_a(t)$, partially reconstructed through the VPR approach. The estimate of EDR through (12) evidences that the strongest peak is around the end of April 16, 2010 with EDR up to 4000 m^3/s, whereas the May event shows peaks less than 300 m^3/s with a more intense activity on May 5, 2010.

3.2 Retrieval spatial maps

The deposited ash at ground during the whole event can be estimated from the retrieved ash fall rate $R_a(\lambda,\phi,z,t)$. By performing a VPR reconstruction, as indicated before, and indicating with $R_a(\lambda,\phi,z=z_s,t)$ the ash fall rate at the surface height, z_s, the spatial distribution of the radar-derived deposited tephra density or loading $D_a(\lambda,\phi)$ [kg m^{-2}] is obtained from:

$$D_a(\lambda,\phi) \equiv \int_{t_i}^{t_f} R_a(\lambda,\phi,z=z_s;t)dt \tag{13}$$

where t_i and t_f are the initial and final time steps of the volcanic eruption. The total space-time deposited tephra mass M_{aT} [kg] from radar measurements can be evaluated by using:

$$M_{aT} = \int_{D_a \geq D_{\min}} D_a(\lambda, \phi) dS \quad (14)$$

where D_{min} is a threshold value of D_a. The radar-derived total ash volume may be estimated by $V_{aT}=M_{aT}/\rho_a$. In order to convert the deposited ash loading D_a into deposited ash depth d_a [m], it holds $d_a=D_a/\rho_a$. Note that M_{aT} could be estimated by integrating (8) as well, but in that case no VPR reconstruction would be performed.

Deposited ash mass $D_a(x,y)$, evaluated through (12) in terms of distal spatial maps derived from radar, can be an appealing way to monitor the evolution of a volcanic eruption in terms of ash fallout as shown in **Fig. 9** and **Fig. 10**. The figures show the accumulated ground mass distribution of the ash within geo-referenced spatial maps, thus providing a useful instrument to gather information about the time progression of the ash fallout. These results indicate that the April volcanic eruption ejected a bigger amount of tephra than that due to the May volcanic eruption.

The sensitivity to the ash category is quite relevant in the radar mass estimation. The latter consideration is confirmed by Fig. 11 and Fig. 12 which, respectively, show the histogram of the 9 radar-estimated ash categories by VARR ash classification (see Table 1) during the whole eruption event and the occurrence of a given ash concentration (small, moderate and intense) within each ash class (fine ash, coarse ash and lapilli). With reference to the whole eruption, the total number of available resolution volumes was 6200376 for April and 5340244 for May, but they have been reduced, respectively, to 121442 and 30423 considering only ash-containing volumes (i.e. excluding all resolution volumes with ash class label value equal to 0). The figures respectively show that, with reference to April, almost 62% of detected ash belongs to coarse ash with moderate concentration (c=5), whereas no bins were labeled as fine ash with small concentration (c=1) nor lapilli with intense concentration (c=9). For the observations in May, above the 85% of total detected ash belongs to coarse ash with small and moderate concentration (c=4 and c=5), whereas there is a low occurence of lapilli (limited to small concentration, with c=7).

Coarse ash particles, as expected, are the most probable with a lower occurrence of finer particles around the volcanic caldera (except fine ash with small concentration). On the contrary, lapilli are found in regions closer to the volcanic vent due to ballistic ejections (note that both on April and May virtually no lapilli have been detected). The occurrences are quite similar in both time windows as shown in **Fig. 11**; coarse ash with small concentration percentage occurrence is higher on May, whereas the fine ash distribution with respect to ash concentration is very similar. Lapilli occurrence is very low on both eruptions. There are two reasons to explain the difference in the total number of ash containing volumes between April and May dataset. First all, the April data refer to one week, whereas the May ones are provided with reference to six days; moreover, the May eruption has been less powerful than the peak of the volcanic activity reached during the month of April and so the number of volumes is not a simple scaling between the two cases of study.

4 Conclusions

The Eyjafjöll explosive volcanic eruptions, occurred on April and May 2010, have been analyzed and quantitatively interpreted by using ground-based weather radar data and VARR inversion technique. The latter has been applied to the Keflavík C-band weather radar, located at a distance of about 155 km from the volcano vent. The VARR methodology has been summarized and applied to available radar time series to estimate the plume maximum height,

ash particle category, ash volume, ash fallout and ash concentration every five minutes. Estimates of the discharge rate of eruption, based on the retrieved ash plume top height, have been also provided together with the deposited ash at ground.

The possibility of monitoring 24 hours a day, in all weather conditions, at a fairly high spatial resolution and every few minutes after the eruption is the major advantage of using ground-based microwave radar systems. The latter can be crucial systems to monitor the "near-source" eruption from its early-stage near the volcano vent, dominated by coarse ash and blocks, to ash-dispersion stage up to hundreds of kilometers, dominated by transport and evolution of coarse and fine ash particles. For distances larger than about several tens of kilometers fine ash might become "invisible" to the radar. In this respect, radar observations can be complementary to satellite, lidar and aircraft observations. Moreover, radar-based products can be used to initialize dispersion model inputs. Due to logistics and space-time variability of the volcanic eruptions, a suggested optimal radar system to detect ash cloud could be a portable X-band weather Doppler polarimetric radar (Marzano et al., 2011b). This radar system may satisfy technological, economical and new scientific requirements to detect ash cloud. The sitting of the observation system which is a problematic tradeoff for a fixed radar system (as the volcano itself may cause a beam obstruction and the ash plume may move in unknown directions), can be easily solved by resorting to portable systems.

Further work is needed to assess the VARR potential using experimental campaign data. Future investigations should be devoted to the analysis of the impact of ash aggregates on microwave radar reflectivity and on the validation of radar estimates of ash amount with ground measurements where available. The last task is not an easy one as the ash fall is dominated by wind advection and by several complicated microphysical processes. This means that what is retrieved within an ash cloud may be not representative of what was collected at ground level in a given area. Spatial integration of ground-collected and radar-retrieved ash amounts may be considered to carry out a meaningful comparison. Preliminary results for the Grímsvötn case study show that the radar-based tephra ash mass estimates retrievals compare well with the deposited ash blanket estimated from in situ ground sampling within the volcanic surrounding area (Marzano et al., 2011a).

Acknowledgements

We are very grateful to B. Pálmason, H. Pétursson and S. Karlsdóttir (IMO, Iceland) for providing C-band radar data and useful suggestions on data processing. The contribution and stimulus of B. De Bernardinis (ISPRA, Italy and formerly DPC, Italy) and G. Vulpiani (DPC, Italy) is gratefully acknowledged. We also wish to thank S. Pavone and S. Barbieri (Sapienza University, Italy) who contributed to the development of the VARR software and the comparison analysis. This work has been partially funded by the Italian Department of Civil Protection (DPC, Rome, Italy) under the project IDRA and by the Sapienza University of Rome (Italy).

References

Ansmann, A., M. Tesche, S. Gro , V. Freudenthaler, P. Seifert, A. Hiebsch, J. Schmidt, U. Wandinger, I. Mattis, D. M uller, and M. Wiegner: The 16 april 2010 major volcanic ash plume over central Europe: EARLINET lidar and AERONET photometer observations at Leipzig and Munich, Germany, Geophys. Res. Lett., L13810, doi:10.1029/2010GL043809, 2010.

Bennett A J, P Odams, D Edwards and Þ Arason: Monitoring of lightning from the April–May 2010 Eyjafjallaj¨okull volcanic eruption using a very low frequency lightning location network", Environ. Res. Lett. 5 , 044013-44022, 2010.

Bonadonna, C., Phillips, J.C., Houghton, B.F.: Modeling tephra sedimentation from a Ruapehu weak plume eruption. J. Geophys. Res. 110, B08209. doi:10.1029/2004JB003515, 2005.

Costa, A., Macedonio, G., Folch, A.: A three dimensional Eulerian model for transport and deposition of volcanic ashes. Earth Planet. Sci. Lett. 241, 634–647, 2006.

Duggen, S., Olgun, N., Croot, P., Hoffmann, L., Dietze, H., Delmelle, P., and Teschner, C.: The role of airborne volcanic ash for the surface ocean biogeochemical iron-cycle: a review, Biogeosciences, 7, 827–844, doi:10.5194/bg-7-827-2010, 2010.

Durant, A. J., Bonadonna, C., and Horwell, C. J.: Atmospheric and environmental impacts of volcanic particulates, Elements, 6, 235–240, 2010.

Flentje, H., H. Claude, T. Elste, S. Gilge, U. Kohler, C. Plass-Dulmer, W. Steinbrecht, W. Thomas, A. Werner, and W. Fricke: The Eyiafjallajokull eruption in April 2010 | detection of volcanic plume using in-situ measurements, ozone sondes and a new generation ceilometer network, Atmos. Chem. Phys. Discuss., 10, 14,947-14,968, 2010.

Gangale, G., Prata, A.J., Clarisse, L., The infrared spectral signature of volcanic ash determined from high-spectral resolution satellite measurements, Remote Sensing of Environment 114 (2), pp. 414-425, 2010.

Gasteiger, J., Groß, S., Freudenthaler, V., and Wiegner, M.: Volcanic ash from Iceland over Munich: mass concentration retrieved from ground-based remote sensing measurements, Atmos. Chem. Phys. Discuss., 10, 26705–26750, doi:10.5194/acpd-10-26705-2010, 2010.

Gertisser, R.: Eyjafjallajokull volcano causes widespread disruption to European air traffic, Geol. Today, 26, 94-95, 2010.

Gouhier M. and F. Donnadieu: Mass estimations of ejecta from Strombolian explosions by inversion of Doppler radar measurements, Journal of Geophysical Research, Vol. 113, B10202, 17 PP., 2008 doi:10.1029/2007JB005383, 2008.

Graf H.-F., M. Herzog, J. M. Oberhuber, and C. Textor, "The effect of environmental conditions on volcanic plume rise," J. Geophys. Res., 104, 20, 24 309–24 320, 1999.

Guðmundsson, M.T., Pedersen, R., Vogfjörð, K., Thorbjarnardóttir, B., Jakobsdóttir, S., Roberts, M. J.: Eruptions of Eyjafjallajökull Volcano, Iceland. EOS 91, 190–191, 2010.

Harris D.M., and W.I. Rose: Estimating particle sizes, concentrations and total mass of ash in volcanic clouds using weather radar", J. Geophys. Res, 88, 10969-10983, 1983.

Kahn, R. A., W.-H. Li, C. Moroney, D. J. Diner, J. V. Martonchik, and E. Fishbein: Aerosol source plume physical characteristics from space-based multiangle imaging, J. Geophys. Res., 112, D11205, doi: 10.1029/2006JD007647, 2007.

Lacasse, C., Karlsdóttir, S., Larsen, G., Soosalu, H., Rose, W. I., and Ernst, G. G. J.: Weather radar observations of the Hekla 2000 eruption cloud, Iceland, Bull. Volcanol., 66, 457–473, 2004.

Larsen, G., Gudmundsson, M. T., Björnsson, H., : Eight centuries of periodic volcanism at the center of the Iceland hotspot revealed by glacier tephrostratigraphy. Geology, 26 (10), 943–946, 1998.

Madonna F., A. Amodeo, G. D'Amico, L. Mona, G. Pappalardo: Observation of non-spherical ultragiant aerosol using a microwave radar, Geophys. Res. Lett., 37, L21814, doi:10.1029/2010GL044999, 2010.

Marzano F.S., E. Picciotti and G. Vulpiani: Rain field and reflectivity vertical profile reconstruction from C-band radar volumetric data, IEEE Trans. Geosci. Rem. Sens., 42, 4, 1033-1046, 2004.

Marzano F.S., G. Vulpiani and W.I. Rose: Microphysical characterization of microwave radar reflectivity due to volcanic ash clouds. IEEE Trans. Geosci. Rem. Sens., 44, 313-327, 2006a.

Marzano, F. S., Barbieri, S., Vulpiani, G.and Rose, W. I.: Volcanic ash cloud retrieval by ground-based microwave weather radar. IEEE Transactions on Geoscience and Remote Sensing, 44, 3235–3246, 2006b.

Marzano F.S., S. Marchiotto, S. Barbieri, C. Textor and D. Schneider, Model-based Weather Radar Remote Sensing of Explosive Volcanic Ash Eruption", IEEE Trans. Geosci. Rem. *Sensing*, vol. 48, pp. 3591-3607, 2010a.

Marzano, F. S., Barbieri, S., Picciotti, E. and Karlsdóttir, S.: Monitoring subglacial volcanic eruption using ground-based C-band radar imagery. IEEE Transactions on Geoscience and Remote Sensing 48, 403–414, 2010b..

Marzano, F.S., M. Lamantea, M. Montopoli, B. Oddsson and M.T. Guðmundsson: Validating subglacial volcanic eruption using ground-based C-band radar imagery, IEEE Transactions on Geoscience and Remote Sensing, submitted, February 2011a.

Marzano, F.S., E. Picciotti, M. Montopoli, and G. Vulpiani: Synthetic Signatures of Volcanic Ash Cloud Particles from X-band Dual-Polarization Radar, IEEE Transactions on Geoscience and Remote Sensing, under revision, February 2011b.

McCarthy, E. B., Bluth, G. J. S., Watson, I. M. and Tupper, A.: Detection and analysis of the volcanic clouds associated with the 18 and 28 August 2000 eruptions of Miyakejima volcano, Japan. International Journal of Remote Sensing, 29(22), 6597-6620, 2008.

Mona, L., A. Amodeo, A. Boselli, C. Cornacchia, G. D'Amico, A. Giunta, F. Madonna, and G. Pappalardo: Observations of the Eyjafjallajokull eruption's plume at Potenza EARLINET station, Geophys. Res. Abs., 12, EGU2010, 15,747, 2010.

Morton, R. R., Taylor, G., F.R.S, Turner, J.: Turbulent gravitational convention from maintained and instantaneous sources. Proceedings of the Royal Society of London. Series A, Mathematical and Physical Sciences, A234, 1–23, 1956.

Oddsson B., M.T. Gudmundsson, G. Larsen and S. Karlsdóttir. Grímsvötn 2004: Weather radar records and plume transport models applied to a phreatomagmatic basaltic eruption.

Proc. IAVCEI (International Association of Volcanology and Chemistry of the Earth's Interior 2008, Reykjavík (Iceland), August 18-24, 2008.

Pavolonis, M.J., Wayne, F.F., Heidinger, A.K., Gallina, G.M.: A daytime complement to the reverse absorption technique for improved automated detection of volcanic ash. Journal Of Atmospheric And Oceanic Technology 23, 1422–1444, 2006.

Pedersen R and Sigmundsson F.:Temporal development of the 1999 intrusive episode in the Eyjafjallajökull volcano, Iceland, derived from InSAR images. Bull Volcanol., 68, 377–393 DOI 10.1007/s00445-005-0020-y, 2006

Petersen, G. N.: A short meteorological overview of the Eyjafjallajokull eruption 14 April till 23 May 2010, Weather, 65, 203-207, 2010.

Pietruczuk, A., J. W. Krzy scin, J. Jaroslawski, J. Podg orski, P. Sobolewski, and J. Wink: Eyjafjallajokull volcano ash observed over Belsk (52° N, 21° E) Poland, in April 2010, Int. J. Remote Sensing, 31, 3981-3986, 2010.

Prata, A. J. and Tupper, A.: Aviation hazards from volcanoes: the state of the science, Nat. Hazards, 51, 239–244, 2009.

Robock, A.: Volcanic eruptions and climate, Rev. Geophys., 38, 191–219, 2000.

Rose, W. J. and Durant, A. J.: Fine ash content of explosive eruptions, J. Volcanol. Geoth. Res., 186, 32–39, 2009.

Sauvageot H., Radar meteorology, Artech House, Boston (MA), 1992.

Schumann, U., B. Weinzierl, O. Reitebuch, H. Schlager, A. Minikin, C. Forster, R. Baumann, T. Sailer, K. Graf, H. Mannstein, C. Voigt, S. Rahm, R. Simmet, M. Scheibe, M. Lichtenstern, P. Stock, H. R uba, D. Schauble, A. Taerner, M. Rautenhaus, T. Gerz, H. Ziereis, M. Krautstrunk, C. Mallaun, J.-F. Gayet, K. Lieke, K. Kandler, M. Ebert, S. W. A. Stohl, J. Gasteiger, H. Olafsson, and K. Sturm: Airborne observations of the Eyjafjalla volcano ash cloud over Europe during air space closure in April and May 2010, Atmos. Chem. Phys. Discuss., 10, 22,131-22,218, 2010.

Sparks R. S. J., M. I. Bursik, S. N. Carey, J. S. Gilbert, L. Glaze, H. Sigurdsson, and A. W. Woods, Volcanic Plumes. New York: Wiley, 1997.

Sparks, R.: The dimensions and dynamics of volcanic eruption columns. Bulletin of Volcanology 48, 3–15, 1986.

Stohl, A., Hittenberger, M., and Wotawa, G.: Validation of the Lagrangian particle dispersion model FLEXPART against large scale tracer experiment data, Atmos. Environ., 32, 4245–4264, 1998.

Stohl A., A. J. Prata, S. Eckhardt, L. Clarisse, A. Durant, S. Henne, N. I. Kristiansen, A. Minikin, U. Schumann, P. Seibert, K. Stebel, H. E. Thomas, T. Thorsteinsson, K. Tørseth, and B. Weinzierl, Determination of time- and height-resolved volcanic ash emissions for quantitative ash dispersion modeling: the 2010 Eyjafjallajökull eruption, Atmos. Chem. Phys. Discuss., 11, 5541–5588, 2011.

Thordarson, T., Larsen, G.: Volcanism in Iceland in historical time: Volcano types, eruption styles and eruptive history. Journal of Geodynamics, 43 (1), 118–152, 2007.

Yu T., W. I. Rose, and A. J. Prata, Atmospheric correction for satellite based volcanic ash mapping and retrievals using split-window IR data from GOES and AVHRR, J. Geophys. Res, vol. 107, no. D16, 4311, 2002.

Wen S. and W.I. Rose: Retrieval of sizes and total masses of particles in volcanic clouds using AVHRR bands 4 and 5, J. Geophys. Res, 99, 5421-5431, 1994.

Wilson, L., Explosive volcanic eruptions - Part II: The atmospheric trajectories of pyroclasts, Geophys. J. R. Astron. Soc., vol. 30, no. 2, pp. 381-392, 1972.

Wilson, L., Sparks, R. S. J., Huang, T. C., Watkins, N. D.: The control of volcanic column heights by eruption energetics and dynamics. Journal of Geophysical Research 83 (83), 1829–1836, 1978.

Zehner, C., Editor: Monitoring Volcanic Ash from Space. Proceedings of the ESA-EUMETSAT workshop on the 14 April to 23 May 2010 eruption at the Eyjafjoll volcano, South Iceland. Frascati, Italy, 26-27 May 2010. ESA-Publication STM-280. doi:10.5270/atmch-10-01, 2010.

TABLES AND FIGURES

Table 1. Ash classes features in terms of average ash diameter $<D_n>$ and concentration $<C_a>$. The variability within each class is Gaussian with a deviation proportional to the mean, $\sigma_{D_n}=0.2<D_n>$ and $\sigma_{C_a}=0.5<C_a>$.

ASH CLASSES	*Light concentration* $<C_a>=0.1\ g\ m^{-3}$	*Moderate concentration* $<C_a>=1.0\ g\ m^{-3}$	*Intense concentration* $<C_a>=5.0\ g\ m^{-3}$
Fine ash size $<D_n>$ = 0.006 mm	**FA-LC c=1**	**FA-MC c=2**	**FA-IC c=3**
Coarse ash size $<D_n>$ = 0.064 mm	**CA-LC c=4**	**FA-MC c=5**	**CA-IC c=6**
Lapilli particle size $<D_n>$ = 0.583 mm	**LP-LC c=7**	**LP-MC c=8**	**LP-IC c=9**

Table 2. Total mass and total volume values for the April 14-20, 2010 eruption period, obtained from radar-derived ashfall rate R_a by selecting a fall velocity values a_v and b_v, derived from the Harris and Rose (1983) ash fallout (HAF) data and the Wilson (1972) ash fallout (WAF) data. Sensitivity of total mass volume to the standard deviation of estimated ashfall rate, indicated by $\sigma(R_a)$, is also shown.

Source	***Fallout model***	***Total mass [kg]***	***Total volume [m^3]***
VARR using R_a-$\sigma(R_a)$	HAF	$8.2455\ 10^{10}$	$6.8713\ 10^{7}$
VARR using R_a	HAF	$8.5193\ 10^{10}$	$7.0994\ 10^{7}$
VARR using R_a+$\sigma(R_a)$	HAF	$8.7734\ 10^{10}$	$7.3112\ 10^{7}$
VARR using R_a-$\sigma(R_a)$	WAF	$6.7303\ 10^{10}$	$5.6086\ 10^{7}$
VARR using R_a	WAF	$7.0193\ 10^{10}$	$5.8494\ 10^{7}$
VARR using R_a+$\sigma(R_a)$	WAF	$6.3656\ 10^{10}$	$5.3046\ 10^{7}$

Table 3. Same as in Table 1, but for the May 05-10, 2010 eruption period.

Source	***Fallout model***	***Total mass [kg]***	***Total volume [m^3]***
VARR using R_a-$\sigma(R_a)$	HAF	$1.3901\ 10^{10}$	$1.1584\ 10^{7}$
VARR using R_a	HAF	$1.6693\ 10^{10}$	$1.3911\ 10^{7}$
VARR using R_a+$\sigma(R_a)$	HAF	$1.2056\ 10^{10}$	$1.0047\ 10^{7}$
VARR using R_a-$\sigma(R_a)$	WAF	$1.0813\ 10^{10}$	$9.0107\ 10^{6}$
VARR using R_a	WAF	$1.2789\ 10^{10}$	$1.0658\ 10^{7}$
VARR using R_a+$\sigma(R_a)$	WAF	$8.7011\ 10^{9}$	$7.2509\ 10^{6}$

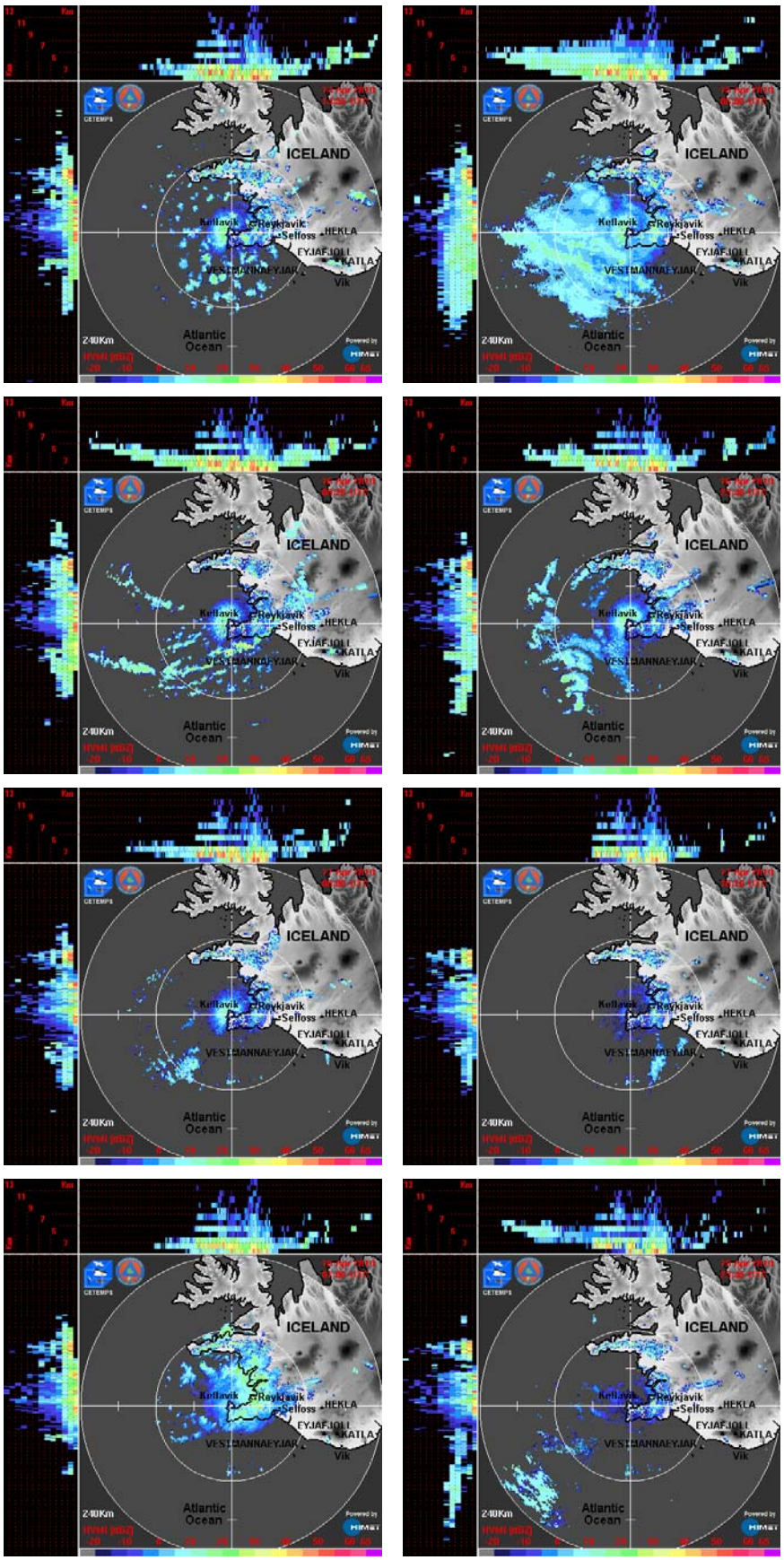

Fig. 1 Eight of the most significant HVMI radar images showing the recorded Keflavík C-band radar reflectivity from April 14, 2010 at 14:55 UTC till April 19 at 23:45 UTC. See text for details.

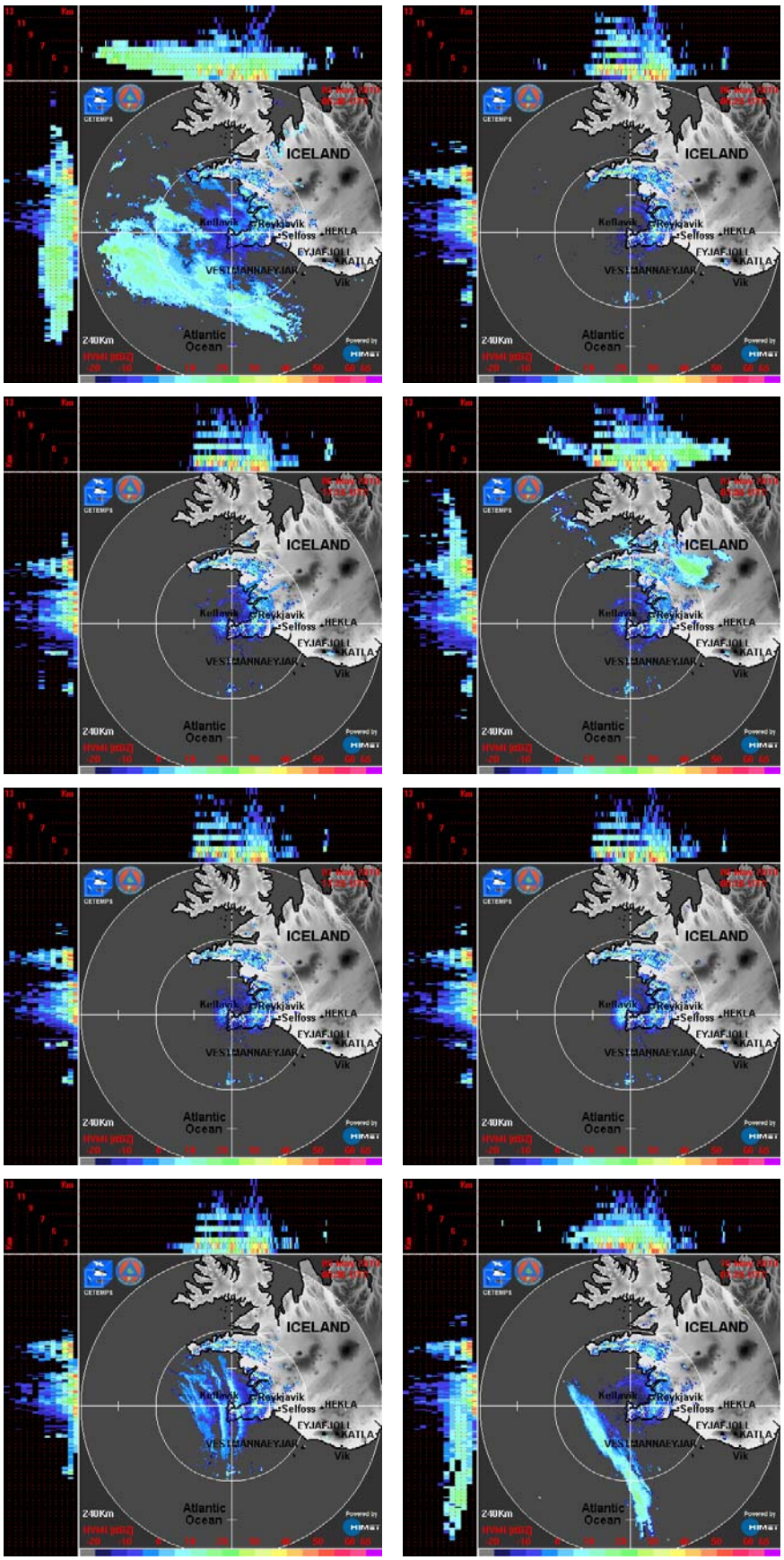

Fig. 2 Eight of the most significant HVMI radar images showing the recorded Keflavík C-band radar reflectivity from May 5, 2010 at 06:40 UTC till May 10 at 01:25 UTC. See text for details.

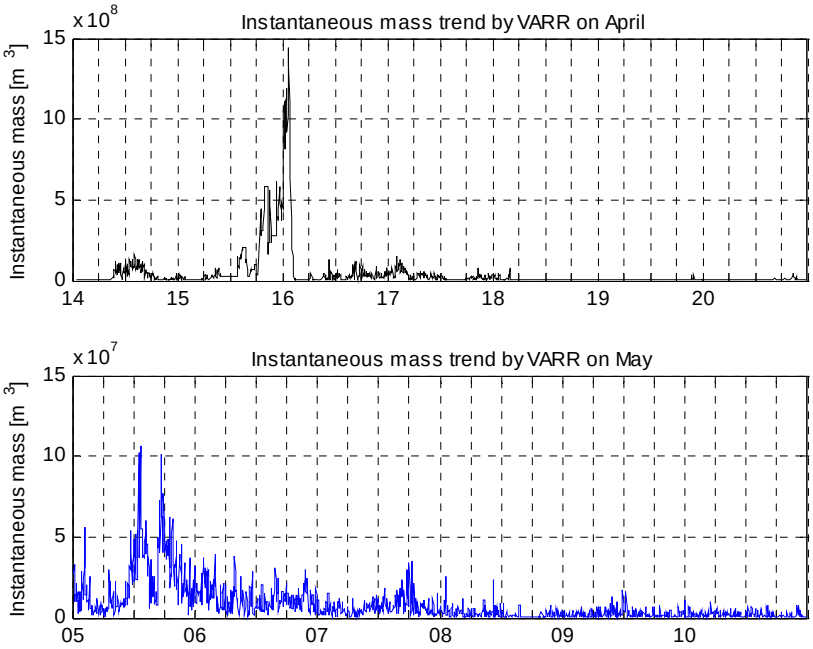

Fig. 3 Instantaneous mass (obtained from ash rate R_a estimated by VARR) versus time expressed in terms of scan days with reference to the eruptions on April (upper panel) and May (lower panel). The ticks on the x-axis have a spacing equal to six hours. The scan sampling period is equal to 5 minutes so that the time series shows a time window of about 10020 minutes (equal to 167 hours) since the first available radar data at 01:00 UTC on Apr 14, 2010 with reference to the dataset of April and about 8630 minutes (equal to 143.8 hours) since the first available radar data at 00:10 UTC on May 5, 2010 with reference to the dataset of May.

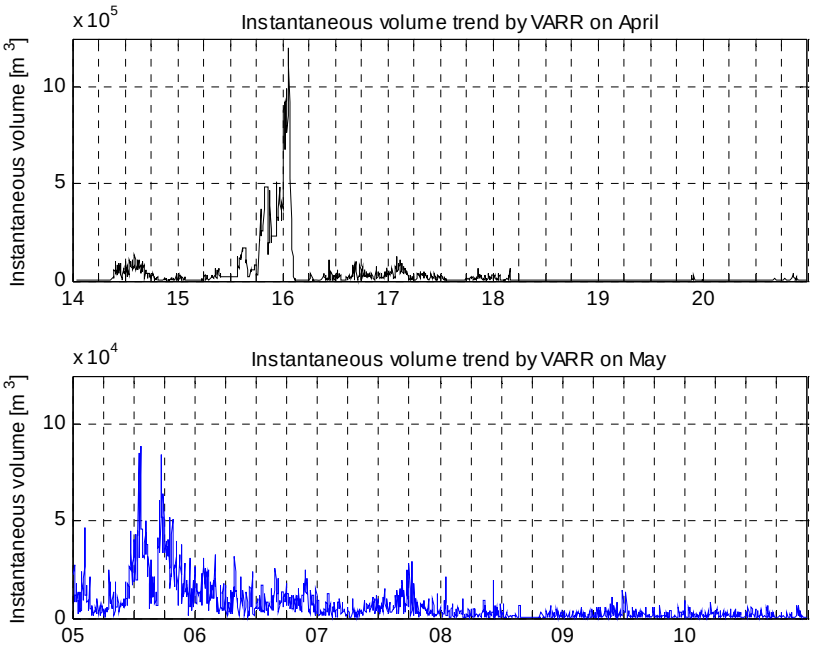

Fig. 4 Instantaneous volume versus scan days, with input data from VARR algorithm with concentration threshold (C_a>10^{-6} kg/m^3). In the upper panel, the trend with reference to April time window (since 01:00 UTC on April 14, 2010 till 23:55 UTC on April 20, 2010); in the lower panel, the trend with reference to May time window (since 00:10 UTC on May 05, 2010 till 23:55 UTC on May 10, 2010).

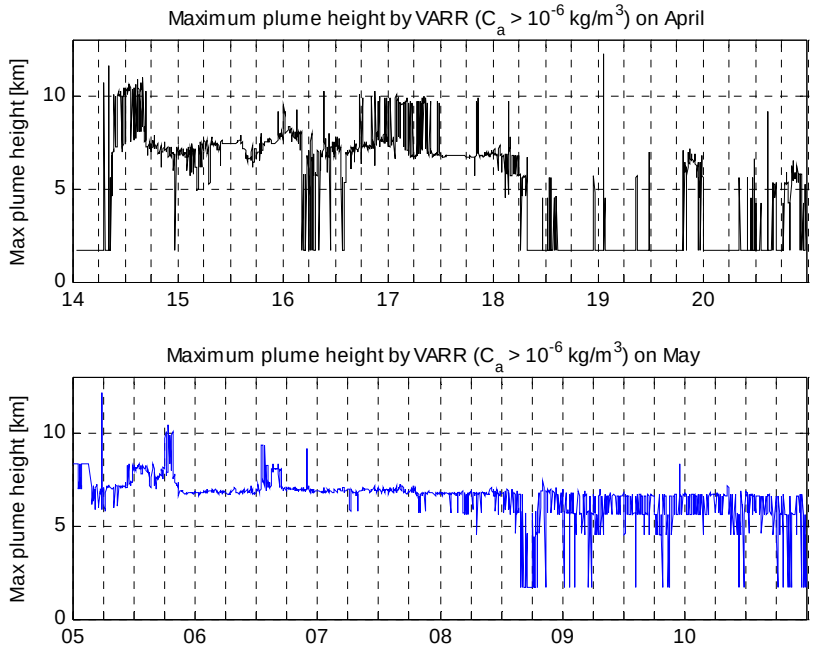

Fig. 5 Instantaneous maximum plume height versus scan days, with input data from VARR algorithm with concentration threshold (C_a>10^{-6} kg/m^3). In the upper panel, the trend with reference to April time window (since 01:00 UTC on April 14, 2010 till 23:55 UTC on April 20, 2010); in the lower panel, the trend with reference to May time window (since 00:10 UTC on May 05, 2010 till 23:55 UTC on May 10, 2010).

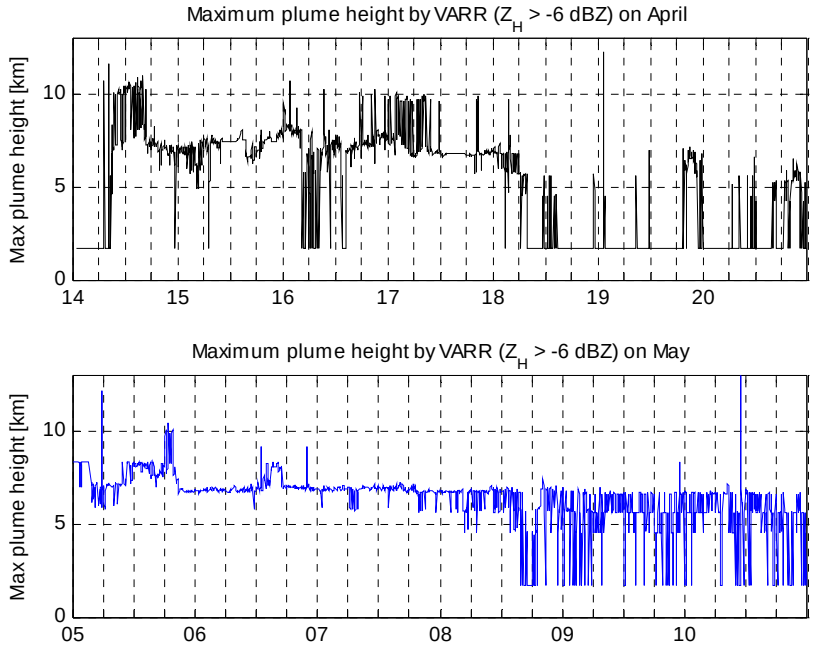

Fig. 6 Instantaneous maximum plume height versus scan days, with input data from VARR algorithm with reflectivity threshold (Z_H>-6 dBZ). In the upper panel, the trend with reference to April time window (since 01:00 UTC on April 14, 2010 till 23:55 UTC on April 20, 2010); in the lower panel, the trend with reference to May time window (since 00:10 UTC on May 05, 2010 till 23:55 UTC on May 10, 2010).

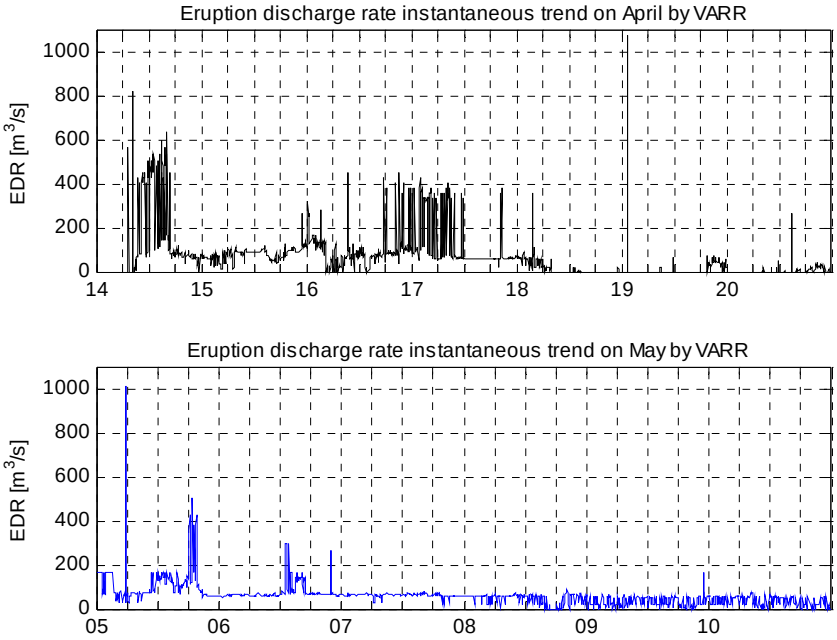

Fig. 7 Instantaneous discharge rate of eruption (EDR), obtained from the maximum plume height versus scan number, with input data from VARR algorithm with concentration threshold (C_a>10^{-6} kg/m^3). In the upper panel, the trend with reference to April time window (since 01:00 UTC on April 14, 2010 till 23:55 UTC on April 20, 2010); in the lower panel, the trend with reference to May time window (since 00:10 UTC on May 05, 2010 till 23:55 UTC on May 10, 2010). Mean EDR values are also quoted in both panels.

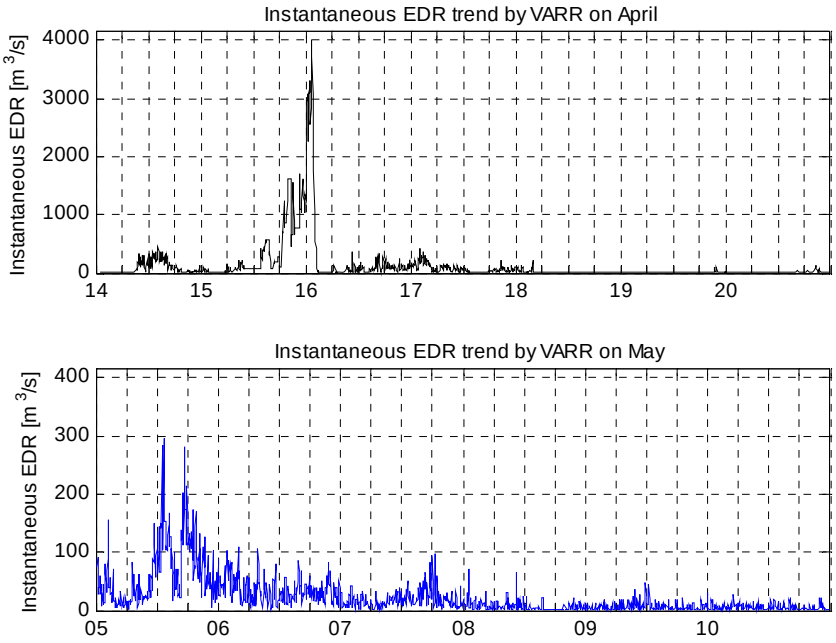

Fig. 8 Same as in Fig. 7, but for EDR derived from the estimated instantaneous ash volume.

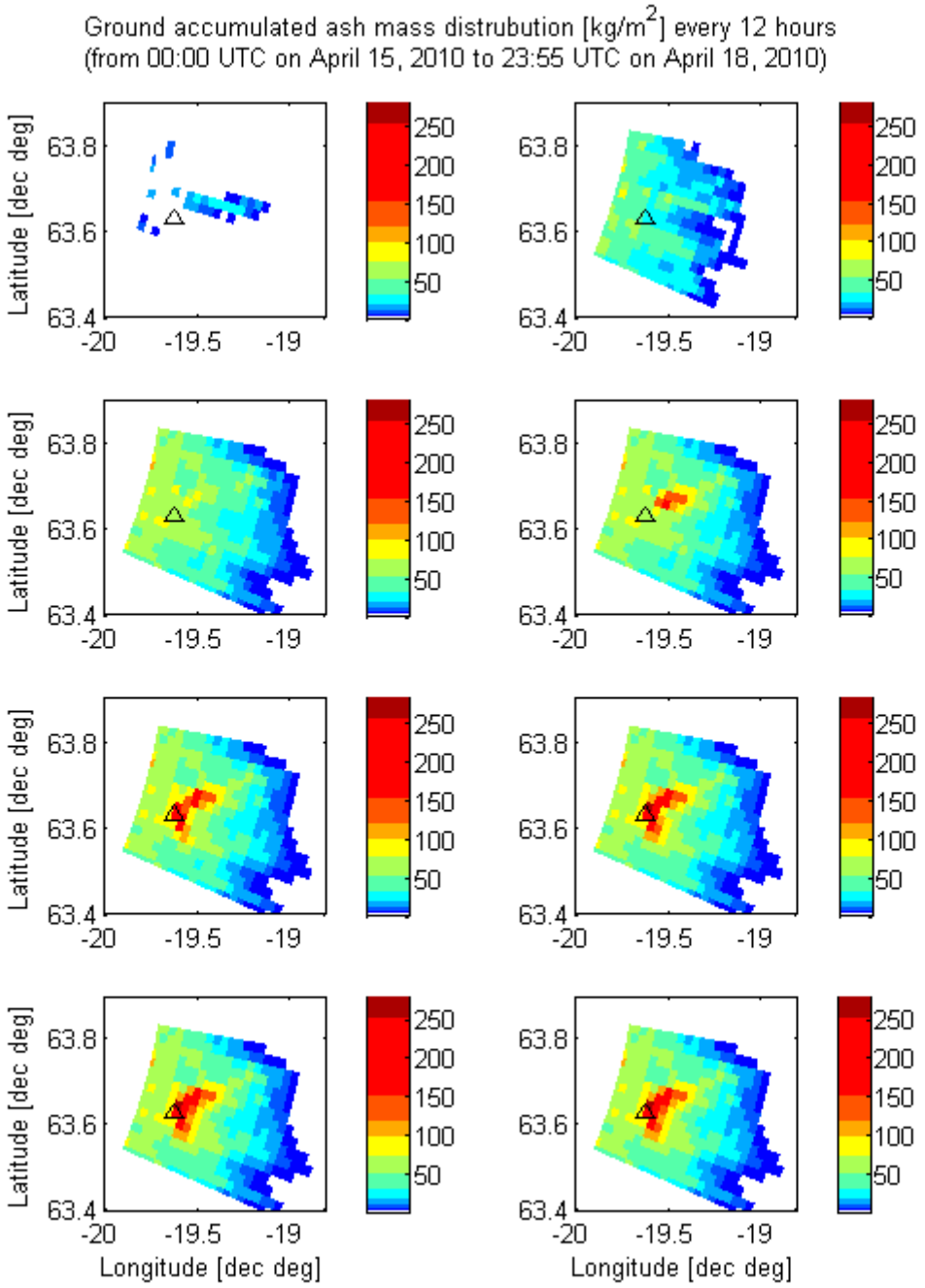

Fig. 9 Distal fallout spatial maps retrieved by VARR. The distributions show the accumulated ash mass at the ground every twelve hours (from left to right, from top panel to bottom) since 00:00 UTC on April 15, 2010 till 23:55 UTC on April 18, 2010. The black edged triangle is centred in the exact position of the Eyjafjöll volcano, whereas colorbars are scaled to match the different dynamic range of the distributions.

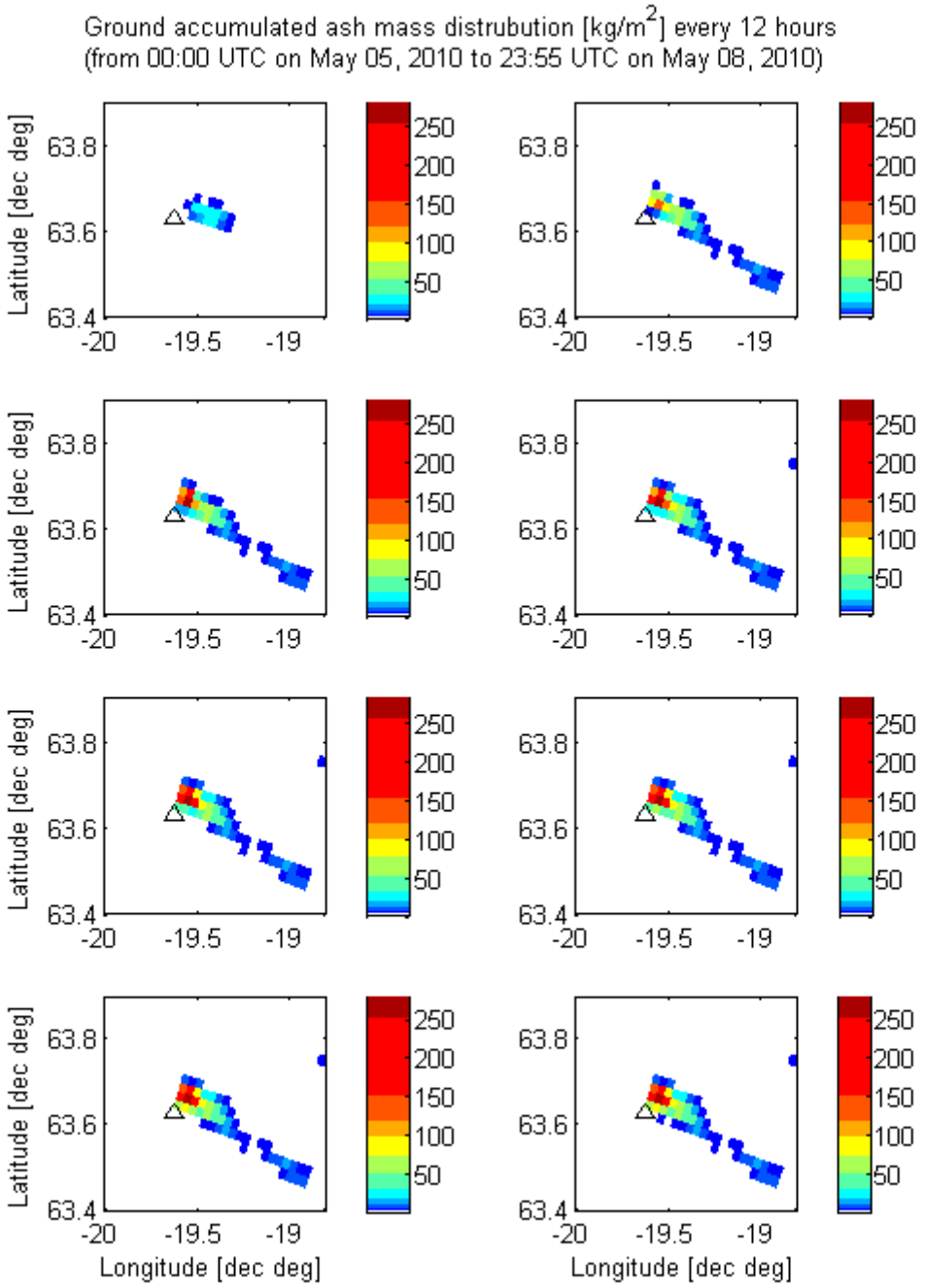

Fig. 10 Distal fallout spatial maps retrieved by VARR. The distributions show the accumulated ash mass at the ground every twelve hours (from left to right, from top panel to bottom) since 00:00 UTC on May 05, 2010 till 23:55 UTC on May 08, 2010. The black edged triangle is centred in the exact position of the Eyjafjöll volcano, whereas colorbars are scaled to match the different dynamic range of the distributions.

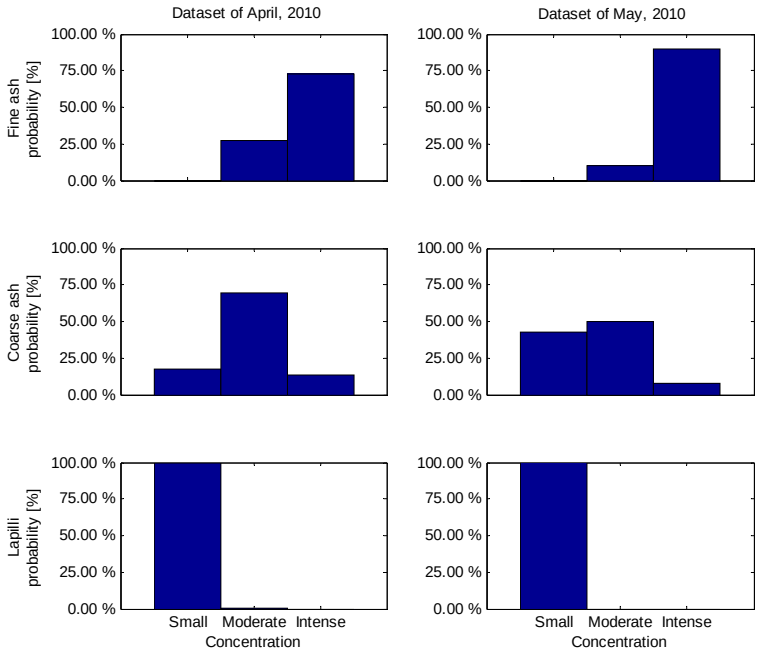

Fig. 11 Histograms showing the probability of a given ash concentration value, with respect to the total number of labels attached to the processed unit radar volumes (121442 for April and 30423 for May) and to the ash class. The latter are displayed on panels from top to bottom as fine ash, coarse ash and lapilli. Only significant volumes have been considered, with reference to the whole eruption since 01:00 UTC on April 14, 2010 till 23:55 UTC on April 20, 2010 (left panels) and since 00:10 UTC on May 5, 2010 till 23:55 UTC on May 10, 2010 (right panels). Note that very few lapilli were detected during the eruptions.

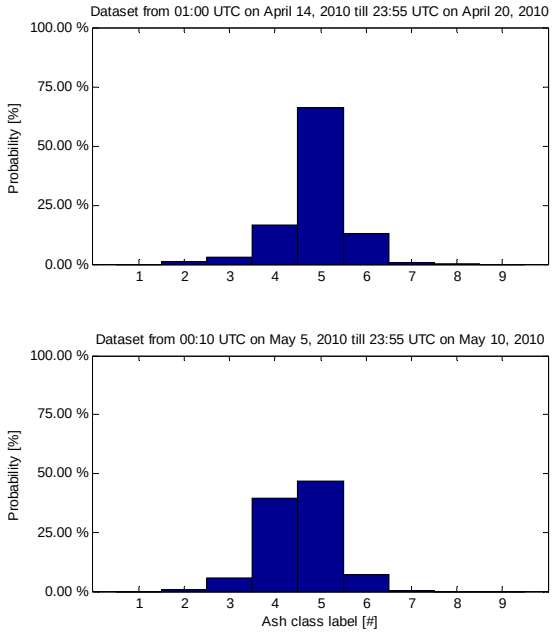

Fig. 12 . Histogram showing the probability of a given ash class label value, with respect to the total number of labels attached to the processed unit radar volumes (121442 for April and 30423 for May). Only significant volumes have been considered, with reference to the whole eruption since 01:00 UTC on April 14, 2010 till 23:55 UTC on April 20, 2010 and since 00:10 UTC on May 5, 2010 till 23:55 UTC on May 10, 2010. Both on April and May, higher occurrence corresponds to coarse ash with moderate concentration, whereas lapilli and fine ash with small concentration have been virtually not observed during the eruption.